Morphology Control of Hairy Nanopores

Orit Peleg,[†,⊥] Mario Tagliazucchi,[‡,⊥] Martin Kröger,[†] Yitzhak Rabin,[‡,§,*] and Igal Szleifer[‡,*]

[†]Polymer Physics, Department of Materials, ETH Zurich, Wolfgang-Pauli-Strasse 10, CH-8093 Zurich, Switzerland, [‡]Department of Biomedical Engineering, Department of Chemistry and Chemistry of Life Processes Institute, Northwestern University, Evanston, Illinois 60208, United States, and [§]Department of Physics and Institute for Nanotechnology and Advanced Materials, Bar-Ilan University, Ramat-Gan, 52900, Israel. [⊥]These authors contributed equally to this work.

ABSTRACT The properties of polymer layers end-grafted to the inner surface of nanopores connected to solvent reservoirs are studied theoretically as a function of solvent quality and pore geometry. Our systematic study reveals that nanoconfinement is affected by both pore radius and length and that the conformations of the polymer chains strongly depend on their grafting position along the nanopore and on the quality of the solvent. In poor solvent, polymer chains can collapse to the walls, form a compact plug in the pore, or self-assemble into domains of different shape due to microphase separation. The morphology of these domains (aggregates on pore walls or stacked micelles along the pore axis) is mainly determined by the relationship between chain length and pore radius. In other cases the number of aggregates depends on pore length. The presence of reservoirs decreases confinement at pore edges due to the changes in available volume and introduces new organization strategies not available for infinite nanochannels. In good solvent conditions, chains grafted at the pore entrances stretch out of the pore, relieving the internal osmotic pressure and increasing the entropy of the polymers. Our study also addresses the experimentally relevant case of end-grafted chains on the outer walls of the membrane surrounding the nanopore. The effect of these polymer chains on the organization within the nanopore depends on solvent quality. For good solvents the outer chains increase the confinement of the chains at the entrance of the pore; however, the effect does not result in new structures. For poor solvents the presence of the outer polymer layer may lead to changes in the morphology of the microphase-separated domains. Our results show the complex interplay between the different interactions in a confined environment and the need to develop theoretical and experimental tools for their study.

KEYWORDS: nanopore · soft matter · nanoconfinement · competing interactions · microphase separation

New physical phenomena arise when condensed matter is confined to length scales similar to the range of intermolecular interactions.[1−4] From the fundamental point of view, confinement of soft materials in the nanometer regime (nanoconfinement) could lead to interesting behaviors that result from the interactions between physical and chemical forces and system size and shape. For example, the radius of long cylindrical channels controls the extent of confinement, modulating the delicate interplay between interactions. As a result, different morphologies, sometimes quite unexpected,[3] may arise. Confinement plays an important role in other relevant systems in nanotechnology, such as nanopatterned surfaces,[5] as well as in biology, for example in nuclear pore complexes (NPCs).[6]

In this article, we present systematic theoretical studies of the morphological behavior of polymers end-grafted to the inner surface of short nanopores that connect two macroscopic reservoirs (see Figure 1). This geometry enables us to demonstrate the importance of shape and size on polymer nanoconfinement. We will show the nontrivial interplay between conformational statistics and geometry as a function of the quality of solvent, presenting the first predictions, to the best of our knowledge, of solvent-induced microphase separation of polymers end-grafted in nanopores. Our results show that the properties of confined polymers as a function of solvent quality differ dramatically from those reported in previous studies of planar polymer films[4,5,7,8] and of infinite polymer-coated cylindrical nanochannels.[9,10]

Polymer-modified pores are extremely important from the experimental point of view, beyond being a paradigmatic example of how nanoconfinement controls phase behavior. State of the art nanofabrication techniques enable the preparation of solid-state nanopores with diameters and thicknesses of a few nanometers,[11] and thus, in forthcoming years, their chemical functionalization will be developed as a logical next step toward the preparation of responsive nanofluidic devices.[12,13] For instance, the past few years have witnessed the first developments of supramolecular modified synthetic nanochannels and nanopores.[1,2,13] Their potential applications range from analytics[14] to energy transduction.[15,16] The organization of the polymer layer plays a key role in these applications, and therefore it is important to understand their response to different external stimuli. As an example, lithographically patterned nanopores modified with

* Address correspondence to rabinserious@gmail.com, igalsz@northwestern.edu.

Received for review February 21, 2011 and accepted April 27, 2011.

Published online April 27, 2011
10.1021/nn200702u

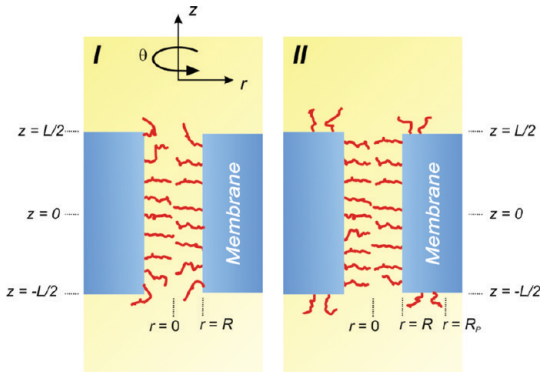

Figure 1. Schematic representation of the two types of cylindrical nanopores considered in this work, including the definition of the coordinate system used throughout. In system I, the inner wall of a single nanopore of radius *R* and length *L* is modified by grafting polymer chains at surface coverage σ. Each polymer molecule contains *N* segments. Each pair of polymer segments interacts through excluded volume repulsions and effective attractive interactions whose strength is measured by the parameter χ (higher χ, stronger segment−segment interactions, lower solvent quality). System II is equivalent to system I, but chains are also grafted on the walls facing the reservoirs (outer walls) up to $r = R_P$.

grafted PEG chains can switch from extended conformations occluding the pore in good solvent (closed pore) to collapsed to the wall conformations in poor solvent (open pore).[17] Modulation of the effective pore cross-section by the collapse to the walls mechanism has been used in the past to explain changes in nanochannel conductivity triggered by solvent quality or temperature changes.[1,18] However, as it is shown here, the collapse of polymer chains to the channel walls is only one of the possible collapse mechanisms for polymers tethered in short nanopores, and the realm of possibilities for control of polymer nanoarchitecture within the pores is very extensive.

Short nanopores with exquisite control of function are found in biology. In eukaryotic cells, the primary translocation pathway for exchange of biomacromolecules between the cytoplasm and the nucleus is through NPCs. These structures are cylindrical nanopores that perforate the nuclear envelope.[19] Intrinsically disordered proteins, the FG-nups, are tethered to the inner surface of the pore. As they interact with potential cargos, the FG-nups are essential to the highly selective translocation mechanism of proteins and of mRNA.[20] Yet, the structural organization of the FG-nups is actively debated, and the field lacks a definitive consensus.[6] In particular, it is not clear how the nanoconfinement affects the spatial distribution of the FG-nups inside the pore and how this in turn is integrated into the translocation mechanism that enables the selective transport of different size proteins.

RESULTS

A distinctive characteristic of the system under study is the presence of several interactions competing on different length scales within a complex geometry. The quality of the solvent is measured by the segment−segment attractive interaction strength χ (larger χ corresponds to higher effective segment−segment attractions and poorer solvent conditions). Attractive interactions favor the formation of dense polymer aggregates, while repulsions and osmotic forces promote swelling of the layer. For polymer−solvent mixtures in solution, strong segment−segment attractions lead to phase separation into a polymer-rich and a polymer-poor phase. However, unlike a polymer solution, irreversibly grafted chains cannot phase separate on macroscopic scales due to the constraint imposed by the grafting (the grafted polymers lack translational degrees of freedom).[7] Therefore, they microphase separate, forming aggregates of high polymer density and varying shapes that, for a planar grafted layer, include micelles, stripes, and holes filled with solvent.[4,21,22] The question that arises is how does the domain formation change due to confinement in nanopores, Figure 1, and how the balance between the different competing interactions and the resulting molecular organization is affected by the geometry, when the pore dimensions are of the same order of magnitude as the characteristic size of the polymers.

Effect of Surface Coverage and Quality of the Solvent. In Figure 2 we present a morphology phase diagram for polymers of different degree of polymerization, *N*, end-grafted to the inner surface of a nanopore (system I in Figure 1), in the plane of quality of solvent (strength of segment−segment interactions, χ) vs surface coverage (σ). The phase diagram also shows color polymer volume fraction maps for each of the different conditions calculated. First, let us consider the thermodynamic manifestation of microphase separation. As mentioned above, the grafted polymers do not have translational degrees of freedom and, therefore, the polymer chemical potential is not a relevant thermodynamic quantity for phase equilibrium. However, the point at which the derivative of the chemical potential of the polymer in the homogeneous layer with respect to the surface coverage becomes negative defines the limit of stability of the homogeneous phase and is an indication of the onset of microphase separation.[4,7] Therefore, we first construct an outline of the phase diagram by determining the onset of microphase separation for the case of an *infinitely* long pore, where we assume that the system can be inhomogeneous only along the radial direction. Correspondingly, the solid lines in Figure 2 give the onset of microphase separation: above the line the system will microphase separate, while below the line the homogeneous phase should be stable. The explicit molecular organization within the pore under different conditions is shown for several different points on the phase diagram. The color maps demonstrate that the prediction for the infinite pore may be used as a useful guideline: self-assembled

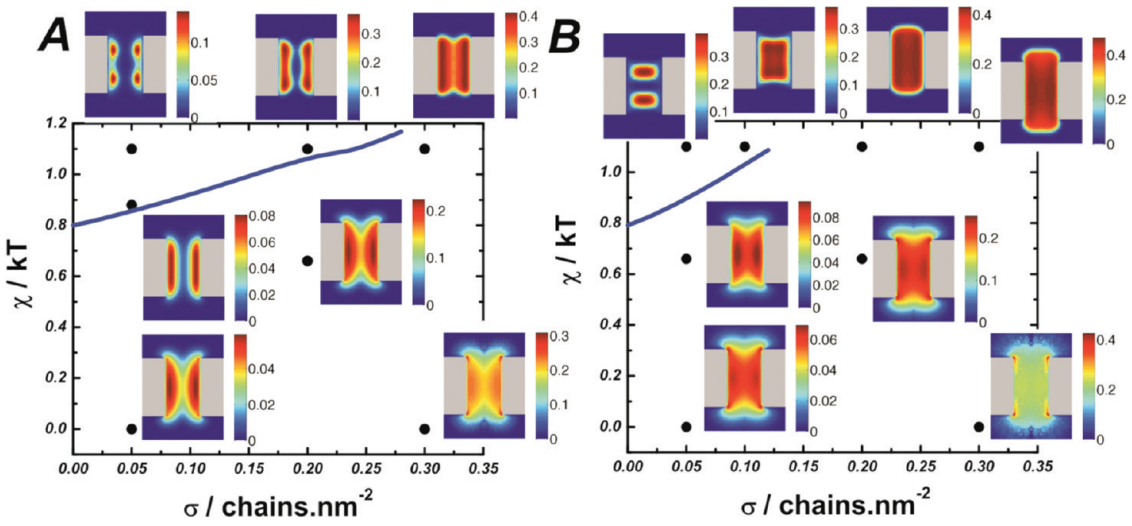

Figure 2. Phase diagram for system I (chains grafted only on the inner walls, $L = 24$ nm, $R = 7.5$ nm) in the interaction strength (χ) grafting density (σ) plane, for polymerization degrees of $N = 45$ (panel A) and $N = 75$ (panel B). Solid lines show the onset of stability for the homogeneous layer in an infinite cylinder as predicted by thermodynamic stability (see text). Polymer volume fraction 2D color maps show the morphologies predicted by the molecular theory at the shown points on the phase diagram. Note that the color scale varies among different maps, in order to emphasize the morphology in each case.

aggregates along the z coordinate appear at high χ and low σ. These microphase-segregated structures can be defined as toroidal (σ = 0.05 chain·nm^{-2}, χ = 1.1 kT, N = 45) or stacked disk-shaped (σ = 0.05 chain·nm^{-2}, χ = 1.1 kT, N = 75) aggregates. At this point, we should note that the assumption of homogeneity in the angular coordinate imposes a limitation on the structures that can form, and therefore, in a real three-dimensional case, one could expect inhomogeneities in θ in addition to those observed for the axial coordinate.[21]

Those states in the diagrams lying below the stability curves correspond to a homogeneous system in z. We should mention that z-homogeneous systems exist only in the case of infinite channels, since in finite pores the presence of the reservoirs breaks the symmetry of the polymer distribution. The terms homogeneous and nonmicrophase-segregated systems are therefore used here in the sense of a system that would present z-independent density profiles for $L = \infty$. Systems with strong segment−segment attractions but outside the instability region present collapsed (but not microphase-segregated) polymer layers with morphologies that depend on the relationship between chain length, surface coverage, and pore radius. For N = 45, the polymer chains collapse to the walls of the pore with practically no polymer density in the reservoirs (σ = 0.3 chain·nm^{-2}, χ = 1.1 kT, N = 45). Nonsegregated systems for N = 75 and χ = 1.1 kT form a uniform and compact plug. At low grafting density, σ = 0.1 chain·nm^{-2}, this plug does not fill the pore completely. However, as σ increases, the size of the plug increases (while the inner polymer volume fraction stays constant around $\langle\phi_P\rangle \approx 0.35-0.45$), and for σ = 0.3 chain·nm^{-2} the ends of the plug are located at the reservoirs. It is clear from these observations that there is an optimal monomer density (which depends on χ) for the collapsed layer, which in this case is around $\langle\phi_P\rangle^{optimal} \approx 0.4$. In other words, long chains collapse to the center of the pore, forming a plug, even when the total number of segments is slightly larger or smaller than that required to reach $\langle\phi_P\rangle^{optimal}$. In those cases, the plug becomes slightly shorter/longer than the pore to compensate for this lack/excess of segments. This is an interesting result that shows how overall optimization is achieved in this complex geometry. The reservoir plays an important role in this organization strategy since it acts as a buffer where the excess of polymer segments can be located, enabling optimal interplay between molecular organization, conformational entropy, and solvent quality.

Decreasing the attractive interaction between segments leads to the good solvent regime. Systems in good solvent ($\chi \approx 0$ kT) and high surface coverage (σ = 0.3 chain·nm^{-2}) exhibit a large number of segments that are expelled from the pore into the two reservoirs. Under these conditions the polymer chains would like to swell as much as possible, and therefore the ability to position a large number of segments within the reservoirs allows minimizing steric interactions between segments and maximizing the conformational entropy of the chains and the translational entropy of the solvent. While for a planar brush the balance between excluded volume interactions and conformational entropy determines the degree of chain stretching,[23] in a short nanopore the confinement imposed by the pore walls introduces a new variable. The number of conformations accessible to a chain located inside the pore will be restricted with respect to those available in the planar case due to the presence of the surrounding wall, *i.e.*, the negative

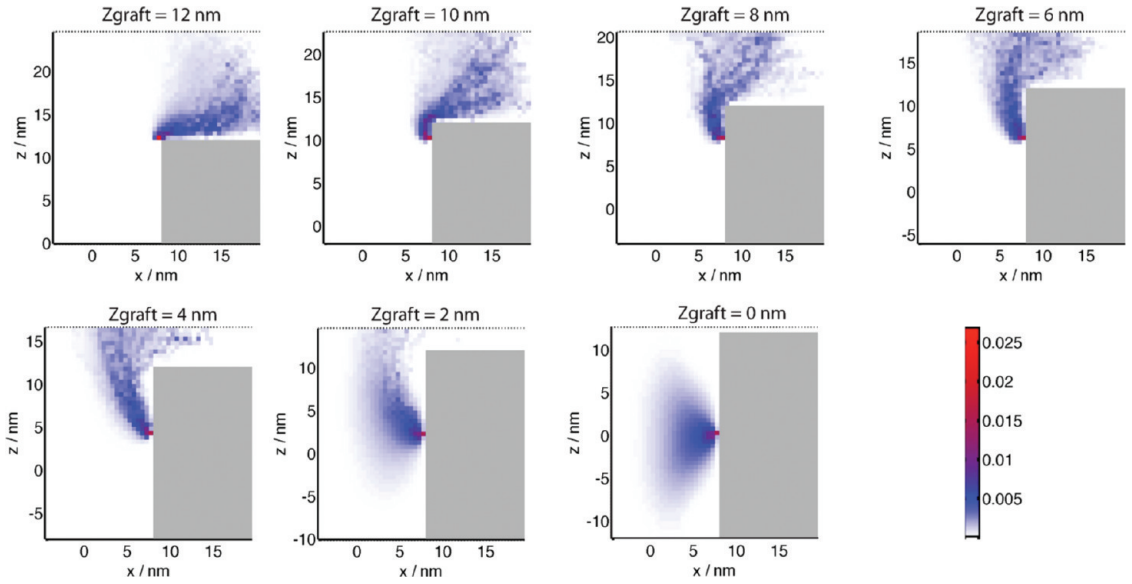

Figure 3. 2D projections of the single chain average segment density in the (*x*, *z*) plane for a chain grafted normal to the *y* axis at different positions (different z_{graft}). The calculations correspond to system I, R = 7.5 nm, L = 24 nm, N = 75, σ = 0.3 chain·nm^{-2}, and χ = 0 kT (good solvent). The grafting positions are marked in the figure. The solid walls of the membrane are shown in gray.

curvature of the grafting surface. While stretching part of the chain so that the remaining segments can get access to the reservoir produces a loss of conformational entropy, these segments now have access to a larger number of configurations, and therefore there is an entropic gain that overcompensates that loss. Therefore stretching the chains toward the reservoir produces a net increase in the conformational entropy. The translational entropy of the solvent (osmotic pressure) increases because relocating the polymer segments to the reservoirs yields a lower polymer (and thus higher solvent) concentration within the pore. The resulting (partial) replacement of polymer by solvent inside the pore increases the overall entropy since confinement imposes a weaker constraint on the free small solvent molecules than on the grafted polymer chains. The increase in polymer concentration outside the pore (increasing the osmotic pressure contribution) is proportionally much smaller, due to the large available volume, than the decrease within the pore (reducing the osmotic pressure contribution).

For N = 45, an inhomogeneous profile is observed in the radial direction (Figure 2A, σ = 0.3 chain·nm^{-2}, χ = 0 kT). On the other hand, N = 75 is long enough that a rather constant density inside the pore is observed. In this case, the reservoir once again plays an important role since the chains close to the entrances are completely stretched out from the pore (σ = 0.3 chain·nm^{-2}, χ = 0 kT, N = 75 in Figure 2B). At this point it is important to emphasize that there are several competing length scales: the dimensions of the pore (R and L), the radius of gyration of the isolated polymer chains (which is a function of the quality of the solvent), the length of the completely stretched chain, and the average distance between grafting points ($\sigma^{-1/2}$). It is therefore not obvious if there is a dominant length scale that determines the behavior of the system. For polymer brushes at high surface coverage on planar surfaces, the height of the layer is linear in the degree of polymerization.[23] However, the nanoscale curvature of the pore surface implies that stretching of the polymers is rather different from the planar case. Furthermore, the geometry implies a highly inhomogeneous stretching of the chains in the different directions, as a function of the quality of the solvent.

The difficulty in identifying the relevant length scale that determines the behavior of the polymers in the nanopore can be observed in the single chain average distribution of segments for different grafting points. This is shown in Figure 3 for polymers in good solvent. The single chain profiles demonstrate that chains tend to reach the reservoir in order to maximize the degree of swelling. The number of segments outside the pore depends on the distance of the grafting point from the reservoir. Thus, chains grafted close to the reservoir have virtually all their segments out of the pore (note that we have chosen a chain grafted at (x = 7.5 nm, y = 0, z) for this representation). This enables the polymer chain to swell as much as possible, at the cost of orienting a few monomers close to the grafting point (and therefore losing their confomational entropy). It is interesting to note that even when the distance of the grafting point to the reservoir is a substantial portion of the stretched length of the chains, the optimal structure is such that a portion of the chain is stretched (the one close to the grafted end) in order to maximize the conformational entropy (swelling) of the other portion of the chain. Only chains grafted in the middle of the

pore (for the given dimensions in the example) have all of their segments within the pore. The single chain profiles in Figure 3 also show that chains that reach the reservoir have a finite density close to the pore edges. The sum of the contributions from different grafting distances produces the small region of very high segment density just at the corner of the channel that is observed in the volume fraction color maps (*i.e.*, in Figure 2B for $\sigma = 0.3$ chain·nm^{-2}, $\chi = 0$ kT, $N = 75$).

Changing the quality of solvent results in a qualitative change of the role of the reservoir, as can be seen in the phase diagram, Figure 2, and in the individual chain profiles displayed in Figure 4. While in good solvent the chains at pore edges escape the channel even at relatively low surface coverages (Figure 4A, $\sigma = 0.05$ chain·nm^{-2}, $\chi = 0$ kT, $N = 75$), in poor solvents polymers grafted around the edge of the pore (Figure 4B, $\sigma = 0.05$ chain·nm^{-2}, $\chi = 1.1$ kT, $N = 75$) are collapsed into the channel due to the strong polymer−polymer attractions. In the microphase-segregated regime (Figure 4B), chains tethered at the center of the pore, $z = 0$, present an average segment distribution that contributes to the two aggregates in the system. This is an interesting situation where the chains, in the equilibrium conditions, have equal probability of belonging to each one of the aggregates. The presence of a region with zero polymer density between the aggregates may impose kinetic limitations on the exchange of chains between domains, which can lead to interesting dynamical properties in the collapsed, segregated films.

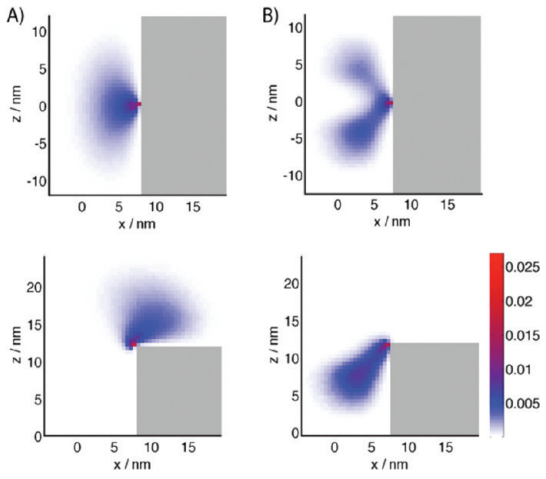

Figure 4. 2D projections of the single chain average segment density, on the (*x*, *z*) planes for two systems shown in Figure 2B (system I, $R = 7.5$ nm, $L = 24$ nm, $N = 75$, $\sigma = 0.05$ chain·nm^{-2}), and $\chi = 0$ kT (good solvent, column A) or $\chi = 1.1$ kT (poor solvent, column B). In both panels, chains located at the center (upper row) and the periphery (lower row) of the pore are shown. The solid walls of the membrane are shown in gray.

Effect of Pore Dimensions. The discussion above concentrated on a pore with fixed geometry and variable grafting density, quality of solvent, and chain length. Since the polymer density profile inside and around the hairy pore is the result of having several relevant length scales competing with each other, we now proceed to examine the rich morphologies that arise when we vary the dimensions of the pore and, therefore, change the ratios of polymer length, pore radius, and pore length.

Figure 5A,B shows the color density maps for a variety of pore radii and lengths for $N = 75$, $\sigma = 0.05$ chain·nm^{-2} in good (Figure 5A) and poor (Figure 5B) solvent conditions. Table 1 compiles the absolute

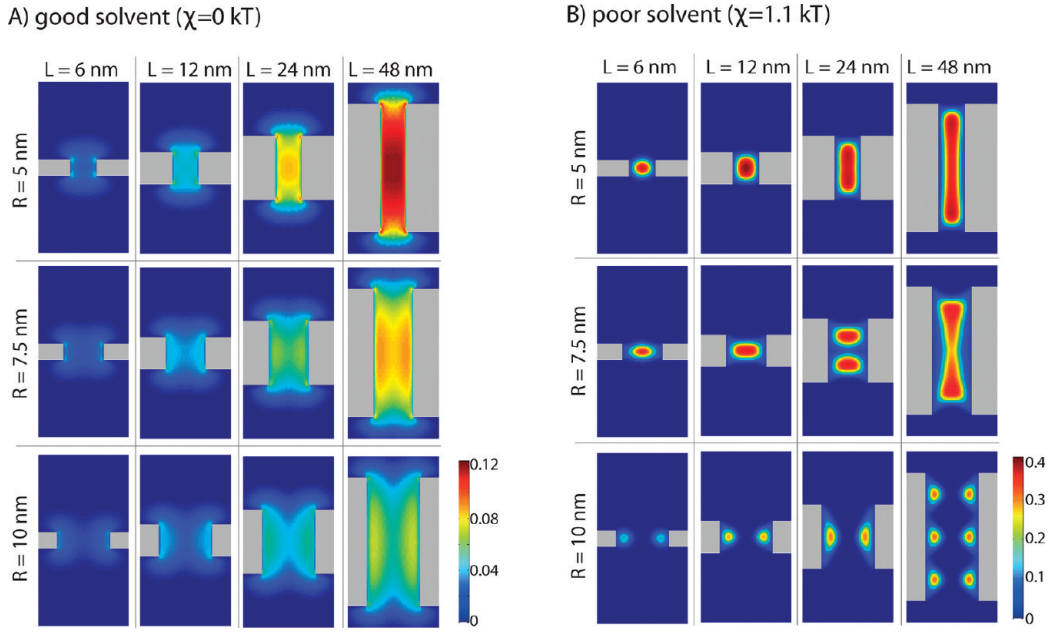

Figure 5. Effect of the pore dimensions on morphology. Polymer volume fraction color maps for system I, $N = 75$, $\sigma = 0.05$ chain·nm^{-2}, and different pore dimensions, as marked in the figure, for (A) good solvent and (B) poor solvent conditions.

TABLE 1. Number and Fraction of Segments Outside the Channel for the Systems in Figure 5

			χ = 0.0 kT		χ = 1.1 kT	
R (nm)	*L* (nm)	total number	% outside	number outside	% outside	number outside
5	6	707	80.2	567	11.01	78
5	12	1414	69.3	980	1.63	23
5	24	2827	50.7	1433	0.4	11
5	48	5655	30	1697	0.2	11
7.5	6	1060	74.3	788	6.92	73
7.5	12	2121	61	1294	0.7	15
7.5	24	4241	42.2	1790	0.32	14
7.5	48	8482	24	2036	0.16	14
10	6	1414	70.4	995	12.03	170
10	12	2827	55.6	1572	0.9	25
10	24	5655	36.6	2070	1.24	70
10	48	11 309	20	2262	0.2	23

number and fraction of segments lying outside the pore (segments at $z > L/2$ and $z < -L/2$) for each case. Increasing length L for fixed radius R in good solvent conditions leads to an increase in the local concentration of segments (note the common color scale for all panels in Figure 5A). In this regime, segments tend to be expelled from the pore in order to maximize the conformational entropy of the chains and to minimize osmotic pressure and polymer repulsions inside the channel. This is easily achieved for short pores; for example for L = 6 nm and R = 5 nm only ~20% of the segments are located inside the channel. For longer pores, the entropic cost associated with stretching chains in order to reach the reservoir becomes too large, and as a consequence the fraction of segments outside the channel decreases with L (see Table 1).

In good solvent conditions, making the pore wider (for fixed L and surface coverage) leads to a decrease of the chain overlap near the pore axis ($r = 0$) and thus to a decrease in the internal polymer volume fraction. As a consequence, the excluded volume repulsion inside the pore decreases and there is no need to stretch the chains out from the channel, and the number of segments in the reservoirs decreases with R (Table 1). Note that the volume of the pore (slice) increases as R^2, while the total number of segments inside the pore for a fixed surface coverage increases as the inner area, *i.e.*, as R. Therefore, as the pore width increases, the chains find more available volume to increase their conformational entropy and reduce the osmotic pressure, without the need to stretch the chains in order to reach the reservoir.

The overlap of chains near the pore axis plays a different and important role in the poor solvent regime, as compared to good solvents. As this overlap is increased by decreasing the radius of the pore, the morphology changes from aggregates on the walls of the system (toroids, R = 10 nm) to in the center (stacked micelles, R = 7.5 nm) until finally a dense plug is formed (R = 5 nm). For high χ values the density of the aggregates (or the plug) does not depend on L, but rather corresponds to the optimal volume fraction for that quality of solvent. Therefore, even for short pores the major fraction of the polymer segment is located inside the channel; see Table 1. For those cases where the system is prone to microphase segregation (*i.e.*, R = 7.5 and 10 nm), the length of the pore determines the number of aggregates that are formed.

The phase diagram for end-tethered polymer layers in good solvent and for an infinite cylindrical pore has been studied by Binder and collaborators using scaling arguments and Monte Carlo simulations.[9,24] Chains much shorter than the pore radius (unperturbed radius of gyration $R_G = (N/6)^{1/2}a \ll R$) exhibit the well-known morphologies for the planar grafted layer: the mushroom and the brush regimes for low and high σ, respectively. For long chains (longer than those used in the present study) and low surface coverage, the polymers are predicted to be in a cigar-like conformation.[9,24] In this regime, chains are elongated in the axial direction in order to avoid the channel walls. This situation imposes an interesting challenge to synthetic methodologies since "grafting to" approaches for such a narrow pore will probably lead to clotting at the entrances.[10] On the other hand, "grafting from" approaches have been shown to be successful in growing polymer brushes within very long and narrow channels,[2] and therefore it is interesting whether the hypothetical cigar-like morphologies can be experimentally addressed with this method. Increasing the surface coverage for narrow channels leads to the compressed cigars and to the overlapping and the compressed brush regimes. From these considerations, the x component of the radius of gyration (R_{Gx}) is predicted to be larger than that in the z (axial) direction (R_{Gz}) when $R \gg N^{1/2}a$ (brush-like regimes, see Figure 6a-ii). On the other hand, for $R \ll N^{1/2}a$, $R_{Gx} \ll R_{Gz}$ (cigar-like regimes, Figure 6a-i). It is intriguing therefore that the chains in Figure 4a ($\sigma = 0.05$ chain·nm^{-2}, $\chi = 0$ kT, and N = 75) are elongated in the z direction, even though they have an unperturbed $R_G = (N/6)^{1/2}a$ = 1.8 nm, much smaller than the pore radius, R = 7.5 nm. In order to understand this result, in Figure 6b we show the different components of R_G as a function of the grafting position (z_{graft}) for R = 10 nm and three different pore lengths (L = 6, 24, and 48 nm). For L = 48 nm, we find that $R_{Gx} > R_{Gz}$ for $z_{graft} = 0$ (pore center), as expected from scaling arguments.

As we discussed above, chains grafted at the pore edges stretch out of the pore in all directions in order to maximize solvent entropy, and thus, for $z_{graft} = -L/2$ and $L/2$ the three components of R_G present rather similar values. This organization creates extra space inside the pore along the z axis, and thus those chains close to pore entrances (but not exactly on the edges)

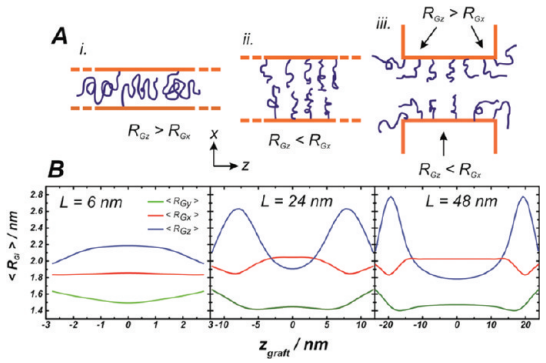

Figure 6. (A) Schematic cartoon for the polymer organization for (i) a cigar-like regime in a very long nanochannel (narrow pore, chains elongated in *z*), (ii) a brush-like regime in a very long nanochannel (broad pore and high σ, chains elongated in *x*), and (iii) a brush-like regime in a short pore. In the latter case, chains are elongated in *x* in the center of the pore and in z close to the ends due to the free space created by the chains protruding into the reservoirs. (B) Predicted components of the radius of gyration as a function of the grafting position (z_{graft}) for pores of different *L*; in all cases $R = 20$ nm, $\chi = 0$ kT, and $\sigma = 0.05$ chain·nm^{-2}.

are elongated along the axial direction. This effect gives rise to the observed maxima in R_{Gz} at $z_{graft} \approx 20$ nm and -20 nm for $L = 48$ nm and at $z_{graft} \approx 10$ nm and -10 nm for $L = 24$ nm. Therefore, the cigar-like shapes in short and wide nanopores arise from the presence of the reservoirs (see cartoon in Figure 6a-iii) that decrease the crowding at the entrances of the pore, allowing the chains close to them to extend in the *z* direction. This is in contrast to the mechanism predicted for long and narrow pores, *i.e.*, a strong confinement in the $x-y$ plane (Figure 6a-i). For a short pore (Figure 6b, $L = 6$ nm), the two R_{Gz} maxima fuse into one centered at $z_{graft} = 0$. In other words, for short nanopores chain conformation is determined not only by the ratio between the unperturbed R_G and R (which is the important parameter for infinite nanochannels) but also by the ratio between the unperturbed R_G and L.

The results of the detailed calculations demonstrate the interplay between the many length scales that are important in determining the behavior of the system and the difficulty of accounting for them by simple scaling arguments. This is particularly important for the nanopores in which some or all of the dimensions are not much larger than the unperturbed size of the polymer chains.

Effect of Grafted Polymers on the Outer Membrane Wall. In Figure 7 we present results for system II (see Figure 1), which has chains tethered to the outer membrane walls in addition to the inner walls. The motivation to study system II is straightforward: it is experimentally easier to modify both the inner and outer part of the membrane than only the inner part (see, for example, ref 25). Depending on the desired application, a synthetic route to selectively graft chains inside the pore may not be required or may not even be desirable. As we have demonstrated above, the presence of the available volume in the reservoir affects the polymer density profile in the pore, and the introduction of additional chains competing for the available volume close to the pore edges should alter the packing in the pore. Even though such effects have been rarely discussed in experimental or theoretical studies, we will demonstrate below that their influence is both important and nontrivial.

For good solvent conditions the effect of the chains grafted to the external surface is to slightly increase the polymer density inside the pore, for both high (Figure 7a) and low (Figure 7b) surface coverage. We showed above that a very important mechanism to relieve the inner osmotic pressure of the pore and to gain overall chain entropy is to stretch the portion of the chains close to the grafting point to enable maximum volume for the rest of the chains by entering into the reservoirs. This effect is partly suppressed by the chains on the outer walls. In other words, chains located at the edge of the pore have a smaller fraction of segments in the reservoirs when other chains are grafted to the outer walls. It is interesting to note the decrease in density on the pore corners for system II (as discussed above for system I, this high-density region arises from stretched chains grafted further away from the entrance). We found that chains grafted at $z_{graft} = 0$ in systems I and II present virtually identical single chain statistics and density profiles (for non-phase-segregated systems). In conclusion, in good solvent conditions the effect of grafted chains on the outer walls on the conformations of the chains grafted inside the pore is similar to that of increasing the length of the pore, since in both cases the confinement of the chains grafted inside the pore is augmented.

In poor solvent conditions and high surface coverage (outside the microphase segregation region), Figures 7c,d, the effect of the chains on the external walls is to decrease the inner density in the pore, opposite to the behavior observed in good solvent. This process occurs because some segments are redistributed from the interior of the pore, where the density is high due to confinement, to the collapsed layer adjacent to the outer walls at the reservoirs. The reason for this behavior is that in the absence of outside polymers the high density inside the pore is obtained at the cost of conformational entropy of the polymers grafted close to the pore entrance. However, the presence of the outer polymers enables those same chains to have a local high density, as needed in the poor solvent regime, without a large conformational entropy cost.

As discussed above, for poor solvent conditions and short chains (*i.e.*, $N = 45$, Figure 7d), the chains collapse to the walls since the entropic penalty for forming a plug in the center is too high. The collapse to the walls mechanism has been recently associated with changes in transport through the pore for stimuli responsive systems.[1,26,27] Our results show that for uncharged

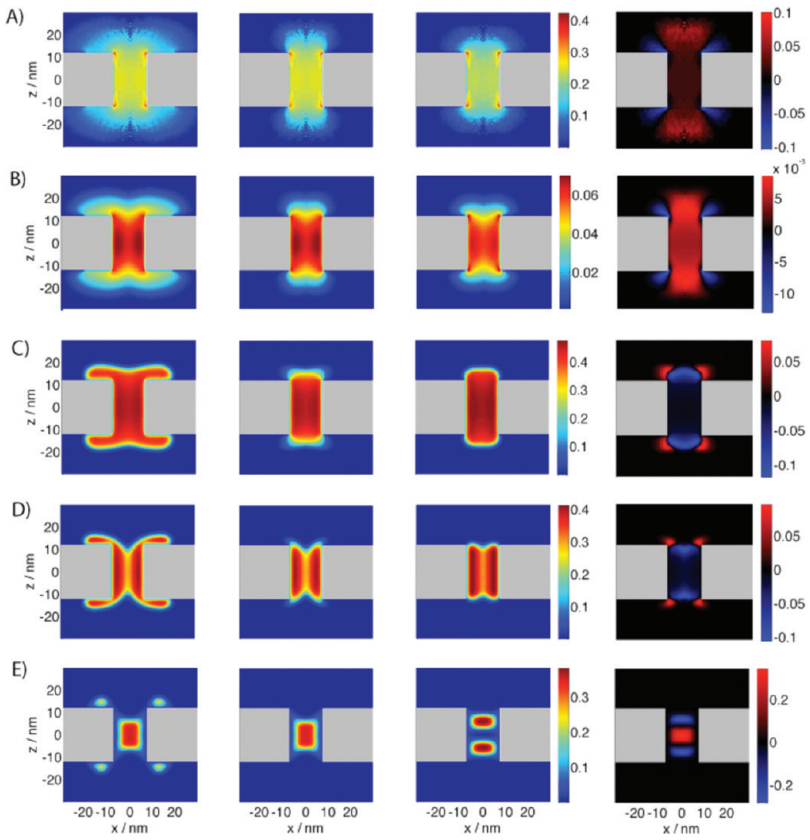

Figure 7. Comparison between polymer morphologies for system II and system I (L = 24 nm, R = 7.5 nm). The first column shows the polymer volume fraction color maps in the case where chains are grafted to both the inner and outer walls (system II). The second column represents the volume fraction of the same system but showing only the contribution of the chains that are grafted to the inner walls of the pore. The third column is for the case of system I, *i.e.*, no polymers grafted outside the pore, for identical conditions to those shown for systems II. The fourth column shows the volume fraction difference between the second and the third columns (*i.e.*, $\Delta\langle\phi_P(\mathbf{r})\rangle = \langle\phi_P(\mathbf{r})\rangle^{\text{system II}} - \langle\phi_P(\mathbf{r})\rangle^{\text{system I}}$) in order to identify regions of increased or decreased density for the polymers grafted within the pore. Calculation conditions: (A) $\sigma = 0.3$ chain·nm^{-2}, $\chi = 0$ kT, $N = 75$, (B) $\sigma = 0.05$ chain·nm^{-2}, $\chi = 0$ kT, $N = 75$, (C) $\sigma = 0.3$ chain·nm^{-2}, $\chi = 1.1$ kT, $N = 75$, (D) $\sigma = 0.3$ chain·nm^{-2}, $\chi = 1.1$ kT, $N = 45$, (E) $\sigma = 0.05$ chain·nm^{-2}, $\chi = 1.1$ kT, $N = 75$.

systems that do not microphase segregate, this mechanism is qualitatively unaffected by grafting chains to the outer walls, and thus the synthetic effort to modify only the inner part of the channels can be avoided. This result may change for charged systems, where it was shown that the surface charge of the outer membrane can affect the ionic conductance of the pore.[28]

Unlike the systems discussed in the previous paragraphs, microphase-segregated layers (low σ, high χ, Figure 7e) may show important qualitative effects due to the presence of grafted chains in the reservoir surfaces. For example, while the system in Figure 7e forms two aggregates when the chains are grafted only on the inner walls of the pore, a single aggregate is formed when the polymers are also tethered to the outer walls. We found, however, that the specific organization is highly dependent on all the parameters, R, L, N, σ, and χ. The main conclusion here is that the optimization strategy that leads to the phase-segregated states is very complex, and therefore, simple arguments cannot predict the observed behavior. There is another interesting physical insight here: after analyzing several combinations of L, R, and R_P we never found aggregates at the pore edge. This result can be understood if we consider that polymer aggregates try to minimize their contact area with the solvent and the walls. Therefore an aggregate in contact with a corner will be disfavored with respect to one lying on a planar surface because of its larger contact area with the membrane. The presence of the polymers grafted to both inner and outer surfaces enables the formation of aggregates on the outer walls, without the need of increasing the surface contacts at the corners.

CONCLUSIONS

In the present work we analyzed the effect of nanoconfinement on the behavior of a polymer layer grafted inside a short pore connecting two reservoirs. The morphological behavior of these systems is very complex and cannot be described by the simple theoretical arguments developed for infinite channels or planar walls. Interesting new phenomena occur at

the pore boundaries, where physical confinement is disrupted and polymer chains tend to escape toward the reservoir in good solvent or to bend into the pore in most poor solvent scenarios. The microphase-segregated regime is of particular interest due to the possibility of creating self-structured materials, as was demonstrated recently for block-copolymer solutions confined inside silica nanochannels.[3] Future theoretical work will be devoted to the study of these aggregates using fully 3D theoretical formalisms accounting for the interactions between electrostatic and chemical equilibria in polyelectrolyte- and polypeptide-modified nanopores.

The functional properties of the pore, its ability to transport small molecules (ions and solvent)[29,30] or large cargos (proteins, DNA, etc),[14,31] are of prime importance for potential applications and for understanding the behavior of biological natural pores, *e.g.*, NPCs. While we have not explicitly addressed these problems here, there are interesting insights that can be gained from our predictions that are relevant for those systems as well. For example, changes in pore conductance with temperature for thermoresponsive polymer-coated pores[1,26,27] have been explained by the collapse of polymer chains on the walls of the pore. In contrast, we have shown here that a broad range of morphological scenarios exists for such systems, that go far beyond the above mechanism. For instance, plug formation will occur for chains with contour lengths longer than pore radius, leading to a decrease of conductance with decreasing quality of solvent (for the noncharged polymer chains discussed here). In the past, the two different mechanisms (collapse to the walls and plug formation) have been used to explain the temperature dependence of conductivity in poly(*N*-isopropylacrylamide)-modified colloidal films.[32] The microphase-segregated regime creates intriguing possibilities for the controlled transport of large cargoes through the pore. For example, the predicted stacked disk morphology in poor solvent consists of polymer-rich plugs along the pore axis, separated by regions of low polymer density. One can envision the case in which sudden changes in the quality of the solvent can lead to trapping (between the plugs) of large molecules diffusing through the channel.

In recent years synthetic tools have been developed to produce a variety of systems with complex shapes and nanoscale dimensions. Competing interactions in those confining geometries lead to organization mechanisms that are not present in simpler, lower dimensional systems. As a consequence, new theoretical tools and physical intuitions will be required for their understanding, and the present work represents a step forward in that direction.

THEORETICAL METHODOLOGY

Our theoretical methodology is an implementation of a previously developed molecular theory for hydrophobic polymers on planar and curved surfaces[33−36] that it is adapted here to the more complex geometry of a short pore connecting two reservoirs. The molecular theory explicitly accounts for the shape, size, and conformational degrees of freedom of all the species in the system and the relevant inter- and intramolecular interactions and van der Waals (vdW) forces.[4,7,33] The basic idea of the theory is to look, for each grafting position **r**, at a very large number of possible polymer conformations and through functional minimization of the free energy obtain the probability for each of those conformations α, $P_P(\mathbf{r}, \alpha)$, depending upon the solution conditions and polymer surface coverage. The predictions of the theory have been found to properly describe structural, thermodynamic, and functional properties of end-tethered neutral and charged polymers as compared with full-scale computer simulations[36,37] and with experimental observations.[4,34,38−40] The theoretical approach is based on writing the free energy functional for the system, *W*,

$$\beta W = \int \rho_s(\mathbf{r})[\ln(\rho_s(\mathbf{r})v_s) - 1]d\mathbf{r} + \sigma \int_A \sum_\alpha P_P(\mathbf{r}(\mathbf{s}), \alpha) \ln (P_P(\mathbf{r}(\mathbf{s}), \alpha) d\mathbf{s}$$
$$+ \frac{\beta\chi}{2} \int \int g(|\mathbf{r}-\mathbf{r}'|)\langle n_P(\mathbf{r})\rangle\langle n_P(\mathbf{r}')\rangle d\mathbf{r}\, d\mathbf{r}' \quad (1)$$

where β = 1/kT. The first term accounts for the translational (mixing) entropy of solvent molecules, with $\rho_s(\mathbf{r})$ and v_s the number density and volume of the solvent molecules, respectively. The second term in eq 1 is the total conformational entropy of the polymer chains, where σ is the polymer surface coverage and the probability of chain conformations $P_P(\mathbf{r}(s), \alpha)$ being normalized at each position on the surface $\mathbf{r}(s)$ (the d*s* integration is over the surface *A* to which the chains are grafted). The last term represents the vdW effective attractive interactions between polymer "beads" (effective chain segments), where $\langle n_P(\mathbf{r})\rangle$ is the number density of polymer segments at **r**, v_P is the polymer segment volume, and $g(|\mathbf{r} - \mathbf{r}'|)$ is a vdW like distance-dependent attractive interaction of the form

$$g(|\mathbf{r}-\mathbf{r}'|) = -\left(\frac{a}{|\mathbf{r}-\mathbf{r}'|}\right)^6$$
$$\text{for } a < |\mathbf{r}-\mathbf{r}'| < 1.5a;\ g(|\mathbf{r}-\mathbf{r}'|) = 0 \text{ otherwise} \quad (2)$$

where *a* is the segment length and 1.5*a* is a cutoff distance (see Supporting Information). Note that the parameter χ (in kT units) in eq 1 measures the strength of the attractive interactions. The intermolecular repulsions are modeled as excluded volume, and they are incorporated on a mean-field level through the packing (incompressibility) constraints,

$$\langle n_P(\mathbf{r})\rangle v_P + \rho_s(\mathbf{r})v_s = 1 \quad (3)$$

where $v_P = 0.095$ nm^3 and $v_s = 0.03$ nm^3 are used throughout, as in ref 4. The equilibrium state of the system is determined by finding the functions $P_P(\mathbf{r}, \alpha)$ and $\rho_s(\mathbf{r})$ that minimize *W* subject to the packing constraints.

In order to allow for a systematic investigation of the phase behavior of the system, we take advantage of the symmetry of the pore and the reservoirs and assume that the system possesses azimuthal symmetry (all the densities and probabilities are independent of θ); that is, we allow only for inhomogeneities in the axial (*z*) and radial (*r*) directions (the minimum number of dimensions needed to model a short nanopore is 2). The coordinate system is explicitly shown in Figure 1. The Supporting Information provides details about the

minimization of eq 1, the generation of the chain molecules, and the methodology used for obtaining the numerical solution of the minimized equations. It is important to stress that the probability $P_P(\mathbf{r}, \alpha)$ in eq 1 is computed by generating a large set of independent conformations of self-avoiding chains that do not intersect the pore walls (for each grafting position). Once these sets are generated, they are used for all the calculations within the same pore geometry, for all the different solvent conditions (for details, see the Supporting Information).

Acknowledgment. This material is based upon work supported as part of the NERC (Non-Equilibrium Research Center), an Energy Frontier Research Center funded by the U.S. Department of Energy, Office of Science, Office of Basic Energy Sciences, under Award Number DE-SC0000989. Y.R. would like to acknowledge the support by grants from the Israel Science Foundation and from the US-Israel Binational Science Foundation. M.K. acknowledges support through research grants ETH-17 10-1and SNF-SCOPES IZ73Z0-128169.

Supporting Information Available: Detailed description of the numerical methods used to solve the molecular theory. This material is available free of charge via the Internet at http://pubs.acs.org.

REFERENCES AND NOTES

1. Yameen, B.; Ali, M.; Neumann, R.; Ensinger, W.; Knoll, W.; Azzaroni, O. Ionic Transport through Single Solid-State Nanopores Controlled with Thermally Nanoactuated Macromolecular Gates. *Small* **2009**, *5*, 1287–1291.
2. Yameen, B.; Ali, M.; Neumann, R.; Ensinger, W.; Knoll, W.; Azzaroni, O. Synthetic Proton-Gated Ion Channels via Single Solid-State Nanochannels Modified with Responsive Polymer Brushes. *Nano Lett.* **2009**, *9*, 2788–2793.
3. Wu, Y. Y.; Cheng, G. S.; Katsov, K.; Sides, S. W.; Wang, J. F.; Tang, J.; Fredrickson, G. H.; Moskovits, M.; Stucky, G. D. Composite Mesostructures by Nano-Confinement. *Nat. Mater.* **2004**, *3*, 816–822.
4. Tagliazucchi, M.; Azzaroni, O.; Szleifer, I. Responsive Polymers End-Tethered in Solid-State Nanochannels: When Nanoconfinement Really Matters. *J. Am. Chem. Soc.* **2010**, *132*, 12404–12411.
5. Jonas, A. M.; Hu, Z. J.; Glinel, K.; Huck, W. T. S. Effect of Nanoconfinement on the Collapse Transition of Responsive Polymer Brushes. *Nano Lett.* **2008**, *8*, 3819–3824.
6. Peleg, O.; Lim, R. Y. H. Converging on the Function of Intrinsically Disordered Nucleoporins in the Nuclear Pore Complex. *Biol. Chem.* **2010**, *391*, 719–730.
7. Gong, P.; Genzer, J.; Szleifer, I. Phase Behavior and Charge Regulation of Weak Polyelectrolyte Grafted Layers. *Phys. Rev. Lett.* 2007, *98*.
8. Advincula, R. C.; Brittain, W. J.; Caster, K. C.; Rühe, J. *Polymer Brushes: Synthesis, Characterization, Applications*; Wiley-VCH: Weinheim, Germany, 2004.
9. Dimitrov, D. I.; Milchev, A.; Binder, K., Polymer Brushes in Cylindrical Pores: Simulation Versus Scaling Theory. *J. Chem. Phys.* 2006, *125*, 034905.
10. Koutsioubas, A. G.; Spiliopoulos, N.; Anastassopoulos, D. L.; Vradis, A. A.; Toprakcioglu, C. Formation of Polymer Brushes inside Cylindrical Pores: A Computer Simulation Study. *J. Chem. Phys.* 2009, *131*, 044901.
11. Dekker, C. Solid-State Nanopores. *Nat. Nanotechnol.* **2007**, *2*, 209–215.
12. Wanunu, M.; Meller, A. Chemically Modified Solid-State Nanopores. *Nano Lett.* **2007**, *7*, 1580–1585.
13. Wen, L. P.; Hou, X.; Tian, Y.; Nie, F. Q.; Song, Y. L.; Zhai, J.; Jiang, L. Bioinspired Smart Gating of Nanochannels toward Photoelectric-Conversion Systems. *Adv. Mater.* **2010**, *22*, 1021–1024.
14. Howorka, S.; Siwy, Z. Nanopore Analytics: Sensing of Single Molecules. *Chem. Soc. Rev.* **2009**, *38*, 2360–2384.
15. van der Heyden, F. H. J.; Bonthuis, D. J.; Stein, D.; Meyer, C.; Dekker, C. Power Generation by Pressure-Driven Transport of Ions in Nanofluidic Channels. *Nano Lett.* **2007**, *7*, 1022–1025.
16. Daiguji, H.; Yang, P. D.; Szeri, A. J.; Majumdar, A. Electrochemomechanical Energy Conversion in Nanofluidic Channels. *Nano Lett.* **2004**, *4*, 2315–2321.
17. Lim, R. Y. H.; Deng, J. Interaction Forces and Reversible Collapse of a Polymer Brush-Gated Nanopore. *ACS Nano* **2009**, *3*, 2911–2918.
18. Adiga, S. P.; Brenner, D. W. Flow Control through Polymer-Grafted Smart Nanofluidic Channels: Molecular Dynamics Simulations. *Nano Lett.* **2005**, *5*, 2509–2514.
19. Alber, F.; Dokudovskaya, S.; Veenhoff, L. M.; Zhang, W.; Kipper, J.; Devos, D.; Suprapto, A.; Karni-Schmidt, O.; Williams, R.; Chait, B. T.; *et al.* The Molecular Architecture of the Nuclear Pore Complex. *Nature* **2007**, *450*, 695–701.
20. Strawn, L. A.; Shen, T.; Shulga, N.; Goldfarb, D. S.; Wente, S. R. Minimal Nuclear Pore Complexes Define Fg Repeat Domains Essential for Transport. *Nat. Cell Biol.* **2004**, *6*, 197–206.
21. Pattanayek, S. K.; Pham, T. T.; Pereira, G. G. Morphological Structures Formed by Grafted Polymers in Poor Solvents. *J. Chem. Phys.* 2005, *122*, 214908.
22. Williams, D. R. M. Grafted Polymers in Bad Solvents - Octopus Surface Micelles. *J. Phys. II* **1993**, *3*, 1313–1318.
23. Alexander, S. Adsorption of Chain Molecules with a Polar Head a-Scaling Description. *J. Phys.* **1977**, *38*, 983–987.
24. Wang, R.; Virnau, P.; Binder, K. Conformational Properties of Polymer Mushrooms under Spherical and Cylindrical Confinement. *Macromol. Theory Simul.* **2010**, *19*, 258–268.
25. Mussi, V.; Fanzio, P.; Repetto, L.; Firpo, G.; Scaruffi, P.; Stigliani, S.; Menotta, M.; Magnani, M.; Tonini, G. P.; Valbusa, U. Electrical Characterization of DNA-Functionalized Solid State Nanopores for Bio-Sensing. *J. Phys.: Condens. Matter* **2010**, 22.
26. Guo, W.; Xia, H.; Xia, F.; Hou, X.; Cao, L.; Wang, L.; Xue, J.; Zhang, G.; Song, Y.; Zhu, D.; *et al.* Current Rectification in Temperature-Responsive Single Nanopores. *ChemPhysChem* **2010**, *11*, 859–864.
27. Guo, W.; Xia, H.; Cao, L.; Xia, F.; Wang, S.; Zhang, G.; Song, Y.; Wang, Y.; Jiang, L.; Zhu, D. Integrating Ionic Gate and Rectifier within One Solid-State Nanopore Via Modification with Dual-Responsive Copolymer Brushes. *Adv. Funct. Mater.* **2010**, *20*, 3561–3567.
28. Vlassiouk, I.; Smirnov, S.; Siwy, Z. Ionic Selectivity of Single Nanochannels. *Nano Lett.* **2008**, *8*, 1978–1985.
29. Daiguji, H. Ion Transport in Nanofluidic Channels. *Chem. Soc. Rev.* **2010**, *39*, 901–911.
30. Sparreboom, W.; van den Berg, A.; Eijkel, J. C. T. Principles and Applications of Nanofluidic Transport. *Nat. Nanotechnol.* **2009**, *4*, 713–720.
31. Martin, C. R.; Siwy, Z. S. Learning Nature's Way: Biosensing with Synthetic Nanopores. *Science* **2007**, *317*, 331–332.
32. Schepelina, O.; Zharov, I. Pnipaam-Modified Nanoporous Colloidal Films with Positive and Negative Temperature Gating. *Langmuir* **2007**, *23*, 12704–12709.
33. Nap, R.; Gong, P.; Szleifer, I. Weak Polyelectrolytes Tethered to Surfaces: Effect of Geometry, Acid-Base Equilibrium and Electrical Permittivity. *J. Polym. Sci., Part B: Polym. Phys.* **2006**, *44*, 2638–2662.
34. Carignano, M. A.; Szleifer, I. Pressure Isotherms, Phase-Transition, Instability, and Structure of Tethered Polymers in Good, Theta, and Poor Solvents. *J. Chem. Phys.* **1994**, *100*, 3210–3223.
35. Szleifer, I.; Carignano, M. A. Tethered Polymer Layers: Phase Transitions and Reduction of Protein Adsorption. *Macromol. Rapid Commun.* **2000**, *21*, 423–448.
36. Carignano, M. A.; Szleifer, I. Structural and Thermodynamic Properties of End-Grafted Polymers on Curved Surfaces. *J. Chem. Phys.* **1995**, *102*, 8662–8669.
37. Carignano, M. A.; Szleifer, I. On the Structure and Pressure of Tethered Polymer Layers in Good Solvent. *Macromolecules* **1995**, *28*, 3197–3204.
38. Tagliazucchi, M.; Calvo, E. J.; Szleifer, I. Molecular Theory of Chemically Modified Electrodes by Redox Polyelectrolytes under Equilibrium Conditions: Comparison with Experiment. *J. Phys. Chem. C* **2008**, *112*, 458–471.

39. Gong, P.; Wu, T.; Genzer, J.; Szleifer, I. Behavior of Surface-Anchored Poly(acrylic acid) Brushes with Grafting Density Gradients on Solid Substrates: 2. Theory. *Macromolecules* **2007**, *40*, 8765–8773.
40. Faure, M. C.; Bassereau, P.; Carignano, M. A.; Szleifer, I.; Gallot, Y.; Andelman, D. Monolayers of Diblock Copolymer at the Air-Water Interface: The Attractive Monomer-Surface Case. *Eur. Phys. J. A* **1998**, *3*, 365–375.
41. Tagliazucchi, M.; de la Cruz, M. O.; Szleifer, I. Self-Organization of Grafted Polyelectrolyte Layers Via the Coupling of Chemical Equilibrium and Physical Interactions. *Proc. Natl. Acad. Sci. U. S. A.* **2010**, *107*, 5300–5305.